eman ta zabal zazu
Universidad del País Vasco
Euskal Herriko Unibertsitatea
ZIENTZIA ETA TEKNOLOGIA FAKULTATEA
FACULTAD DE CIENCIA Y TECNOLOGÍA

Bachelor Thesis
Degree in Physics

Coexistence of the Two Dimensional Electron Gas and Ferroelectric Domains in Ferroelectric Thin Films

Abstract

Thin film ferroelectrics screen their in-built depolarizing electric field by forming domains of opposite polarization within the film. Similar materials have been found to favour surface charge accumulation as screening agents for their electrostatic build-up, leading to the formation of two-dimensional electron gas (2DEG) at the interface between the film and the substrate. The thesis explores the possibility of both screening mechanisms coexisting.

Author:
Maitane Muñoz Basagoiti

Directors:
Emilio Artacho
(Theory Group, CIC nanoGUNE)
José María Pitarke
(Department of Theoretical Physics, UPV-EHU)

June 2017 - Leioa

Contents

«Nothing in life is to be feared, it is only to be understood. Now is the time to understand more, so that we may fear less.»

Marie Skłodowska Curie

1 Introduction

The discovery of the formation of the Two-Dimensional Electron Gas (2DEG) at the heterointerface of two insulating oxides (the LAO/STO system) in 2004 opened a new research path in the field of surface phenomena [1]. Over the past couple of years great effort has been devoted to determining the exact origin of this LAO/STO interface of conducting nature, which still today remains unclear and controversial, motivated by the remarkable properties of the LAO/STO interface – magnetic, metallic or superconducting behaviour [2, 3, 4].

Among the many formation mechanisms proposed [3], the theory that stands out is that of the *polar catastrophe*, which states that the driving force for the formation of the electron gas is the polar discontinuity at the interface. Interestingly, since the magnitude of this polar mismatch can be manipulated, the conduting nature of the interface can conviniently be switched on and off. One of the many possible ways of doing so is by using ferroelectric materials where the spontaneous polarization can be used as the source of a 2DEG [5, 6]. However, a ferroelectric thin film has alternative mechanisms to screen the polar discontinuity at the interface other than surface charge accumulation: It can break into ferroelectric domains and cancel the need of a 2DEG to compensate for the polar catastrophe.

Therefore, formation of the 2DEG and ferroelectric domains in ferroelectric thin films have always been considered as mutually exclusive polarity-screening agents and have had the possibility of their coexistence overlooked. Nevertheless, backed by discussions with Matthew Dawber's experimental team[1] and published papers [5], this thesis will explore whether a coexistence region of both mechanisms is actually achievable from a theoretical point of view.

[1] Private Communications.

The objective of the thesis is thus to prove that a coexistence region of surface charge of quasi-two-dimensional nature and domains in ferroelectric thin films actually exists. In order to do so, we will combine the theory for the stabilization of a monodomain phase with a 2DEG in ferroelectrics [5] and the electrostatics of a polydomain ferroelectric system [25] to obtain a phenomelogical Landau-type model. The model will be both analytically – within a few approximations – and numerically solved and the transition from the polydomain state without a 2DEG to the monodomain phase with a 2DEG analysed. Coexistence will be proved if the transition between the two phases is smooth.

The coexistence of a two-dimensional electron gas and a domain pattern structure in ferroelectric thin films would suggest the emergence of quasi-one-dimensional carrier densities with promising future applications and vast phenomenology yet to be both studied and understood.

2 2DEG and Ferroelectricity: State of Art and the Coexistence Hypothesis

Over the last few years, a particular family of oxides has received an enormous amount of attention: perovskites. Perovskites are a form of inorganic crystals whose general formula can be expressed by ABX_3, A and B being cations – A atoms are larger than B atoms – and X, an anion. The ideal cubic unit cell above perovskite's Curie temperature consists of A cations at the edges of the cube $(0,0,0)$, B cations at the centre of the cell $(1/2,1/2,1/2)$ and the X anions – most frecquently oxygen – at face centered positions $(1/2,1/2,0)$ (figure 1). Below Curie temperature, symmetry of the perovskite unit cell is lowered to orthorhombic, tetragonal or trigonal.

Because of their multifunctionality, perovskites stand out as crystallographic hosts for a large range of interesting properties [7] (such as superconductivity [8], ferroelectricity [5] and even magnetic behaviour) and promising technological applications (field effect devices [9], solar cells [10], sensors and detectors for instance). In particular, perovskites are here introduced since they represent the material scenario in which the high carrier mobility [1] ($\sim 10^4\,\mathrm{cm}^2\,\mathrm{V}^{-1}\,\mathrm{s}^{-1}$) two-dimensional electron gas subjected to analysis in this thesis is formed.

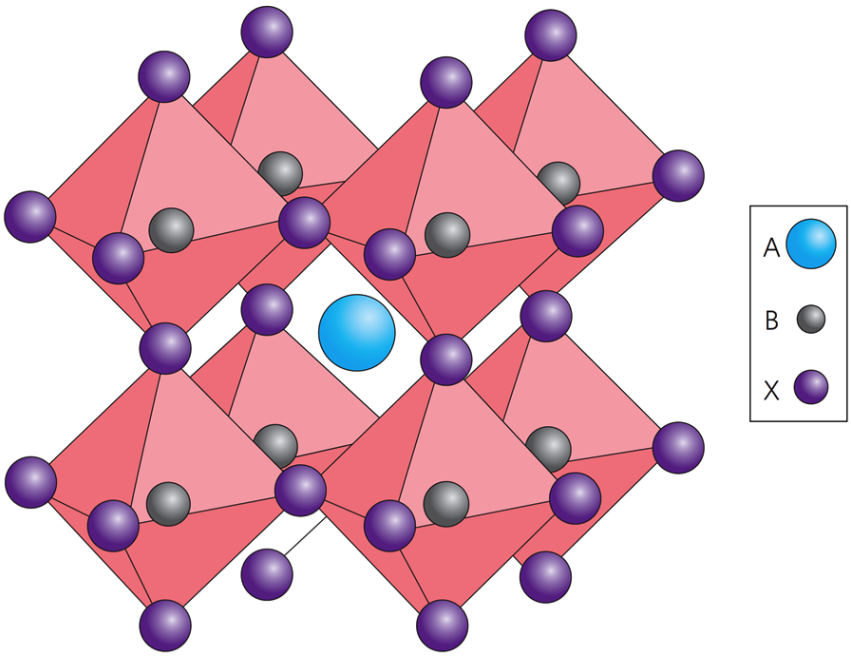

Figure 1: Perovskite crystal structure [10]

2.1 The Two-Dimensional Electron Gas (2DEG)

The discovery of the Two-Dimensional Electron Gas (2DEG) at the interface between two prototypical insulating oxides was first made by Ohtomo and colaborators in 2002, when authors grew an idealized structure of layers of $LaTi^{3+}O_3$ perovskite embedded in $SrTi^{4+}O_3$. By means of an atomic-scale electron beam, they reported [11]:

> '[...] *We hace observed the spatial distribution of the extra electron on titanium sites. This distribution results in metallic conductivity, even though the superlattice structure is based on two insulators.*'

Further research carried out on the LAO/STO ($LaAlO_3/SrTiO_3$) system suggested that polar discontinuities at the interface could indeed originate unsual charge states and non-trivial electronic structure at the heterointerface, exhibiting metallic behaviour of quasi-two-dimensional nature. It was then in the pioneering work published in 2004 when Ohtomo and Hwang showed that «*an unusual, non-bulk like charge state is formed at this* [LAO/STO] *polar interface* » [1]. The 2DEG had been found.

Prospective applications of this highly mobile carrier density at the heterointerface of two perovskite insulators led to a great number of topical reviews [2, 3, 4] and publised research [12, 13], serving these publications as an indication of the big impact the breakthrough had. Nevertheless, although systems giving rise to the 2DEG – either superlattices or film-over-substrate systems – are being extensively studied because of their remarkable properties and technological potential as stated before, the exact origin of this new interphase phenomena remains yet to be fully understood since it is believed that more than one mechanism plays a role in determining the interesting conducting behaviour.

2DEG formation mechanisms proposed so far can be categorised in those based on the intrinsic polar nature of the structure – such as the *electronic reconstruction* phenomenon and surface charge accumulation via *redox screening* [3] – and those based on extrinsic effects and material deffects – such as dopping through trapped *oxygen vacancies* in the surface of the substrate. However, the only proposed model in agreement with all experiments and which is able to account for both conducting and insulating interfaces is that of the electronic reconstruction [12]. This thesis will thus assume the electronic reconstruction mechanism as the base of the 2DEG formation.

It will be shown that polar interfaces can induce intrinsic interface dopping and therefore, be the driving force for the formation of the two-dimensional electron gas. These interface polar discontinuities are not uncommon and can naturally arise in layered oxide structures as ferroelectric titanes or in artificially produced thin film heterostructures. Simple electrostatic arguments enable us to show that net charge at a polar interface leads to an energetically unstable electrostatic potential upon growing sample thickness, a phenomenon referred to as the *polar catastrophe* (figure 2). This polar mismatch at the interface will invoke screening via surface charge accumulation.

2.1.1 Polar Interfaces: The Polar Catastrophe and Electronic Reconstruction

The net surface charge characterizing a polar interface can be understood in terms of the formal charges of the alternating AO and BO_2 planes in which the ABO_3 perovskite structure is divided along the $[001]$ crystallographic direction [14]. The oxygen has

formal valence O^{2-} while A and B cations may take formal charge values

$$A^{4+}B^{2+} \qquad A^{3+}B^{3+} \qquad A^{2+}B^{4+} \qquad \text{or} \qquad A^{1+}B^{5+},$$

making the ABO_3 structure neutral. Depending on the compound, each of these (001) planes will either be polar (such is the case for $LaAlO_3$, composed of LaO and AlO_2 alternating layers, $+1$ and -1 charge per surface unit for each of them) or neutral (as for $SrTiO_3$, with SrO and TiO_3 alternating neutral planes).

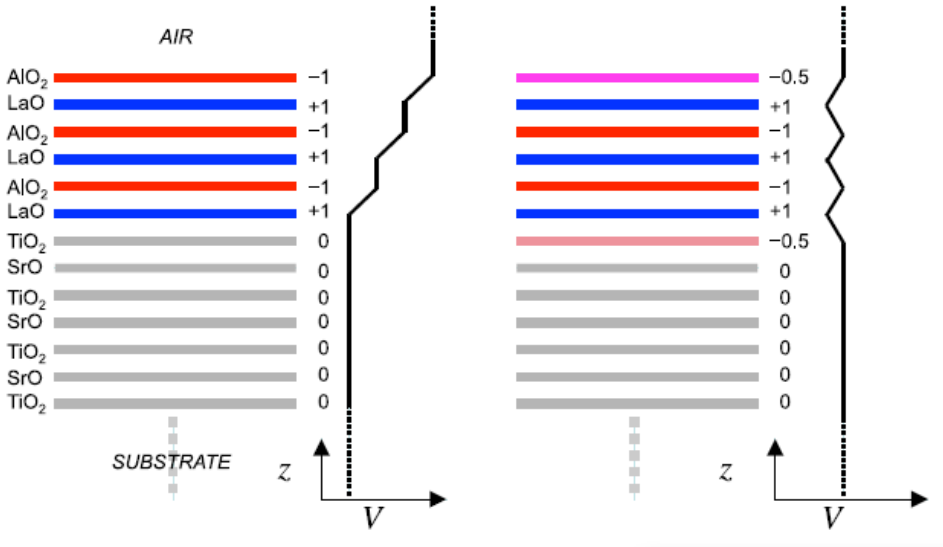

Figure 2: **Left panel**: The polar catastrophe in the LAO/STO system explained in terms of the atomic layers in the [001] crystallographic direction taken as charged planes. **Right panel**: The system is stabilized by transferring half an electron from the surface layer to the interface. From [3].

It is the growth of a particular family of planes over another compound with different formal polarization in the [001] crystallographic direction what leads to a polar discontinuity at the boundary between these two materials. If there is no redistribution of charges at the interface, the electrostatic potential across the perovskite film will diverge with thickness, a phenomenon referred to as the *polar catastrophe*. Deposition of $LaTiO_3$ over $SrTiO_3$ is equivalent to joining capacitors in series. The electrostatic potential across each capacitor is then added, resulting in a divergent potential with the number of capacitors joined, that is, with the LAO film thickness. In the pursuit of system-energy minimization, some form charge compensation may occur at the interface, balancing the diverging electrostatic

potential and giving rise to the 2DEG by means of an *electronic reconstruction*.

The polar nature of the LAO/STO interface lies in a charge imbalance (also referred to as *chemical charge*) of $\pm e/2$ per surface unit, the sign depending on the lattice plane at the interface termination. For a LAO film grown over a STO substrate, interface can either be *n*-type for a TiO_2/LaO heterointerface or *p*-type if it is SrO/AlO_2. It is however the *n*-type interface the one showing the novel conducting properties, while the *p*-type interface is found to be insulating.

In the absence of electronic reconstructions, this chemical charge at the interface per surface unit, $\sigma = e/2$, gives rise to a non-decaying electric field across the LAO film in the [001] direction,

$$E_{LAO} = \frac{\sigma}{\varepsilon} \qquad \text{where} \qquad \varepsilon = \varepsilon_0(1 + \chi_{LAO}), \tag{2.1}$$

and where linear dielectric response for the LAO film,

$$P_{LAO} = \varepsilon_0 \chi_{LAO} E_{LAO} \tag{2.2}$$

is assumed. The electronic reconstruction concept refers to the process by which this electric field across the LAO film induces an electronic transfer. This transfer will take electronic carriers from surface valence band to the conduction band at the interface once the magnitude of the electrostatic potential across the film is equal to the band gap Δ. Electrons then are energetic enough to perform an interband transition. The reconstruction will thus take place when a certain critical thickness d_c of the film layered over the substrate is achieved. Beyond this thickness, carrier density reaches equilibrium and the conductivity linked to highly-mobile carriers can be measured at the interface if this is an *n*-type interface.

2.2 Ferroelectrics

Pyroelectricity is the phenomenon in which temperature variation leads to a change in the polarization of the material, inducing a non-zero electric field along the sample. Crystals whose most stable structure is nonpyroelectric above the Curie temperature T_C and pyroelectric below it are called *ferroelectrics*.

The stable non-polar phase above the Curie temperature is called *paraelectric* phase, while below the Curie temperature the material will be polar and possess a spontaneous polarization – hence the name *ferroelectric* in analogy with ferromagnetic materials, which have a net magnetic moment. This polarization can be reversed through the application of an electric field [24]. In fact, the criterion for ferroelectricity is actually the reversibility of the spontaneous polarization in an attainable applied electric field rather than its mere existence [15].

The transition from the unpolarized to the pyroelectric polarized state can either be first order if the polarization $\vec{P}$ acquires a nonzero value right below T_C, or second (or higher) order if $\vec{P}$ grows continuosly from zero as temperature drops below T_C. For a continuous ferroelectric transition below the Curie temperature, the crystal sample will continuously distort to a polarized state yielding an anomalously large dielectric constant near T_C. This will reflect the vanishing of the restoring force opposing the lattice distortion from the unpolarized to the polarized phase, giving rise to a zero-frequency optical mode known as *soft mode*. This soft mode's polarization vector will describe the distortion and will be adressed later on as the parameter of order when the Landau-type model for the 2DEG formation in ferroelectrics is presented.

What is the motivation behind working with ferroelectric materials to achieve heterointerface conduction phenomena? Ferroelectric materials offer the opportunity of manipulating the electrostatic boundary conditions of the system through their spontaneous polarization. Therefore, these materials can be used as the source for the 2DEG-invoking polar discontinuity.

Ferroelectric polarization can indeed be employed to control the polarization mismatch at the interface and switch on and off the electron gas, an idea which is already being exploited. Aguado-Puente et *al*. showed by first-principle calculations that *«a monodomain ferroeletric phase with a 2DEG can be stabilized in a $PbTiO_3$ film layered over a $SrTiO_3$ substrate »* [5]. The system has gathered a lot of attention and motivated further research [6]. However, the main challenge ferroelectric materials pose is that although its switchable polarization may lead to the formation of the 2DEG, it is by no means the single alternative the material possesses to counteract the energetically unstable electrostatic build-up: the ferroelectric material can also break into polarization domains.

2.2.1 Ferroelectric screening mechanisms: Domains and the Kittel-Mitsui-Furuichi (KMF) formula

A ferroelectric material may choose an alternative route to avoid the polarization mismatch at the interface between the film and the sustrate. In the absence of an external macroscopic electric field, the stable configuration of the ferroelectric thin film will be determined by the thickness d of the sample. Although single-domain states are found energetically favorable for thick enough films [5], bound charges on the surface – originated by the spontenous ferroelectric polarization – may render this configuration unstable. In fact, these charges are responsible for the *depolarazing electric field*, which is opposed to the spontaneous polarization of the sample and has a high energetic cost. The system may then break into polarization domains and give rise to complex domain patterns to counter the energy related to the depolarizing electric field.

Ferroelectric equilibrium domain patterns correspond to system energy minima when the sample harmonizes its intrinsic properties and external conditions. Successful treatments of equilibrium domain structures in ferromagnets [17, 18] led to research in domain patterns in ferroelectric samples in thermodynamic equilibrium. The models presented in this thesis will be focusing on the so-called 180° domains: each domain contains antiparallel orientation of the uniaxial spontenous polarization vector as shown in figure 3, the domain width being w.

If the ferroelectric sample splits into domains to minimize the electrostatic energy due to the depolarazing field, there is an additional contribution to the total energy of the system: the domain wall energy, which will be proportional to the density of domains formed and the film thickness. Thus, the system must find the equilibrium between the energetic cost of the depolarazing electric field and domain wall formation, consequently evolving towards a ferroelectric polydomain state or remaining in the monodomain phase. Nevertheless, paraelectric configuration might also be a stable phase of the system.

The depolarizing field can be neglected for thick enough films since it rapidly decays with thickness. Therefore, the monodomain phase is to be expected as the stable configuration of the system in the thick film limit. Thin films, where the depolarizing field is no longer negligible, are expected to be broken into the multidomain state.

First proposed by Kittel for magnetic systems [18] and then extended for ferroelectrics by Mitsui and Furuichi when discussing domain patterns in Rochelle salt crystals [19], the Kittel-Mitsui-Furuichi (KMF) law establishes the relation between the ferroelectric domain width or domain pattern period w and the sample thickness d by balancing the energy contributions of the domain walls and the depolarazing field. It theoretically predicts that ferroelectric domain width w grows with the square root of the sample thickness,

$$w \propto \sqrt{d} \tag{2.3}$$

This simple result is obtained by minimizing the total energy of the system: the electrostatic energy due to the depolarizing field and the energy cost related to the formation of domain walls in the polydomain ferroelectric state.

$$U_{Total} = U_{dep} + U_W \tag{2.4}$$

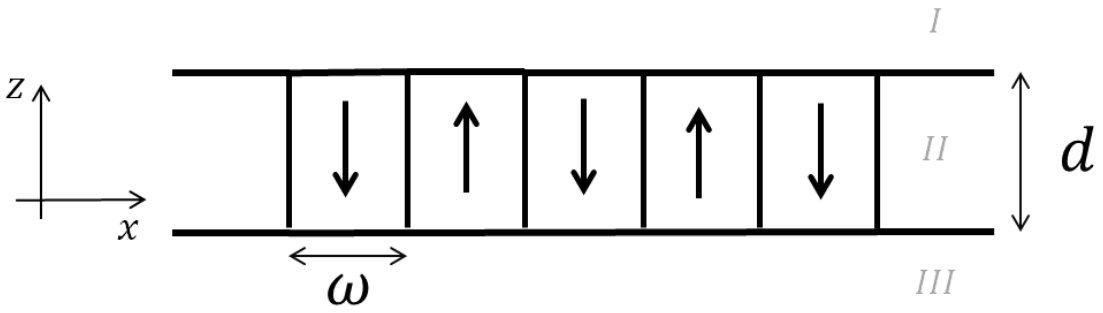

Figure 3: Schematic configuration of the ferroelectric 180° domain pattern.

The electrostatic energy related to the depolarizing field can be computed by first determining the spatial field distribution for the periodic configuration shown in figure 3. In order to perform the calculations, the literary reference followed [25] suggests assuming the sample is behaving as a *hard* ferroelectric, its dielectric response being linear,

$$P_z(x,y,z) = \pm P_S + \varepsilon_0(\kappa_c - 1)E_z(x,y,z) \tag{2.5}$$

$$P_x = \varepsilon_0(\kappa_a - 1)E_x(x,y,z) \tag{2.6}$$

$$P_y = \varepsilon_0(\kappa_a - 1)E_y(x,y,z) \tag{2.7}$$

The electrostatic potential is obtained by solving the Laplace and Poisson equations for all three regions in space - I, II and III -, where I and III are vacuum.

The spatial density of the depolarizing field electrostatic energy is then given by the familiar relation:

$$\Phi_{dep} = \frac{1}{2}\vec{E}(\vec{D} - \vec{P}_s) = \frac{1}{2}\varepsilon_0 \kappa_{ij} E_i E_j \tag{2.8}$$

which is computed for the 180° domain pattern configuration. The electrostatic energy per unit volume for a system as shown in figure 3 is finally given by the convergent series [25],

$$U_{dep} = \frac{8P_s^2}{\pi^3 \varepsilon_0}\frac{w}{d}\sum_{n=1}^{\infty}\frac{1}{n^3}\sin^2\left(\frac{n\pi}{2}\right)\frac{1}{1+\sqrt{\kappa_a\kappa_c}\coth\left(\frac{n\pi}{2}\sqrt{\frac{\kappa_a}{\kappa_c}}\frac{d}{w}\right)} \tag{2.9}$$

The parameters κ_a and κ_c are the components of the dielectric tensor in the transversal and longitudinal directions. This last expression correspondingly simplifies to the electrostatic energy for a regular capacitor for thick enough ferroelectric films ($x = d/w \ll 1$) when the monodomain phase is expected,

$$\lim_{w \gg d} U_{dep} \to \frac{P_s^2}{2\varepsilon_0 \kappa_c} \tag{2.10}$$

The second contribution to the total energy (2.4), the energy due to the formation of domain walls, is directly proportional to ferroelectric domain density: the larger the number of domains formed, the larger the amount of walls. Therefore, the cost of domain wall formation decreases with the domain pattern period and it can be expressed as (in units per volume),

$$U_W = 2\frac{\Sigma}{T} = \frac{\Sigma}{w} \tag{2.11}$$

where Σ is wall energy per unit surface and w is half the domain pattern period or simply the domain width. Minimization of the total energy density (2.4) with respect to domain width w with film thickness d fixed leads to the classical square-root Kittel-Mitsui-Furuichi law (2.3).

2.3 Screening Mechanism Competition and the Analysis of the Coexistence

The equilibrium configuration of a system is always attained by lowering its energy in the pursuit of a more stable state. The formation of the two-dimensional electron gas at polar interfaces and the multidomain state in the ferroelectric bulk material are both mechanisms that allow the system to lower its energy by screening energetically unstable electrostatic potentials.

However, even though ferroelectrics have extensively been studied with regards to their usefulness in tuning the interface polarity and potentially induce the 2DEG, both 2DEG formation and ferroelectric domains have always been regarded as mutually exclusive screening agents, consequently neglecting the possibility of both mechanisms coexisting[2].

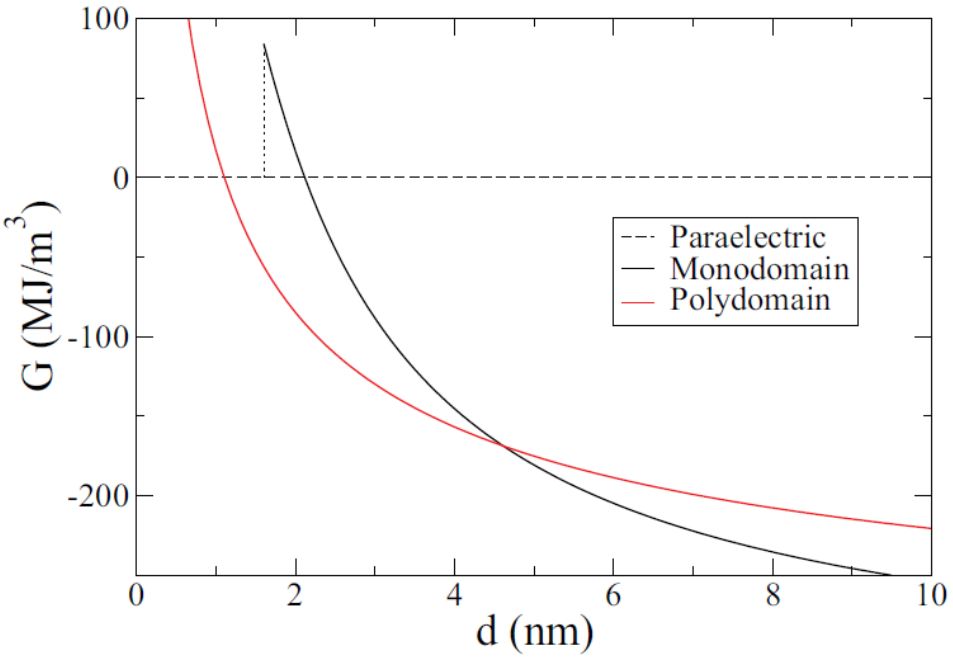

Figure 4: Ferroelectric thin film energy density for the monodomain (black) and polydomain state (red) obtained from [5].

[2]In April 2017, while this thesis was being written, a manuscript was published in `arxiv.org` suggesting the coexistence of ferroelectric domains and surface charge accumulation as screening agents for the first time [20].

Since the equilibrium configuration of the system will depend on film thickness d, the sample will transition from polydomain to monodomain phase as d grows. Figure 4, obtained from Aguado-Puente's *ab-initio* studies on the PTO/STO system [5], shows a comparison between the energy density for both monodomain and polydomain phases, emphasizing the theoretical predictions made above: it will be energetically more favourable for the system to be broken into domains in the thin film limit whereas the monodomain phase stabilized by a 2DEG is the most favorable scenario above a certain critical thickness.

As the plot 4 suggests, each phase – monodomain or polydomain – prevails for a particular range of thickness d values and a crossover between the two phases is to be expected. However, Aguado-Puente's model, which will be introduced in subsequent sections, considers the formation of the 2DEG and ferroelectric domains as independent screening mechanisms. Therefore, if his model were to be reformulated by simultaneously considering the formation of the 2DEG and ferroelectric domains, would the crossover between polydomain and monodomain phases still be a sharp transtion or a coexistence of the two-screening mechanisms is to be expected?

Discussion with Matthew Dawber and the experimental data obtained by his team[3] reinforced the possibility of both aforementioned screening mechanisms coexisting. Based on that, the hypothesis this thesis presents is that the crossover between the two phases and prevalence of one of the mechanisms over the other, depending on the ferroelectric film thickness, might actually be a *coexistence region*: ferroelectric domains witness the formation of the 2DEG and altogether evolve (that is, domain pattern period increases while surface charge accumulates) with film thickness until domain width w diverges giving way to the monodomain stable phase with a 2DEG.

Schematic representations of the core idea of the thesis are presented in figures 5 and 6. As intends to be shown, there will be a range of film thicknesses for which the 2DEG will combine with ferroelectric domains to minimize system energy, forming complex quasi-one-dimensional carrier structures, namely 1DEG stripes that would cover the ferroelectric sample.

[3] Private Communications.

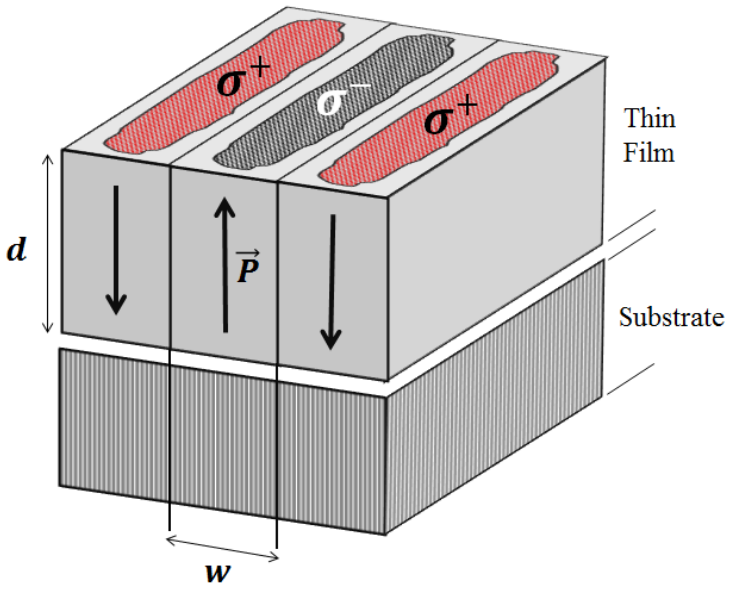

Figure 5: Schematic representation of the studied system in the coexistence region: the ferroelectric thin film is split into domains and two-dimensional electron (2DEG) and hole (2DHG) gases appear at the surface and interface of the film depending on the orientation of the polarization in the domain.

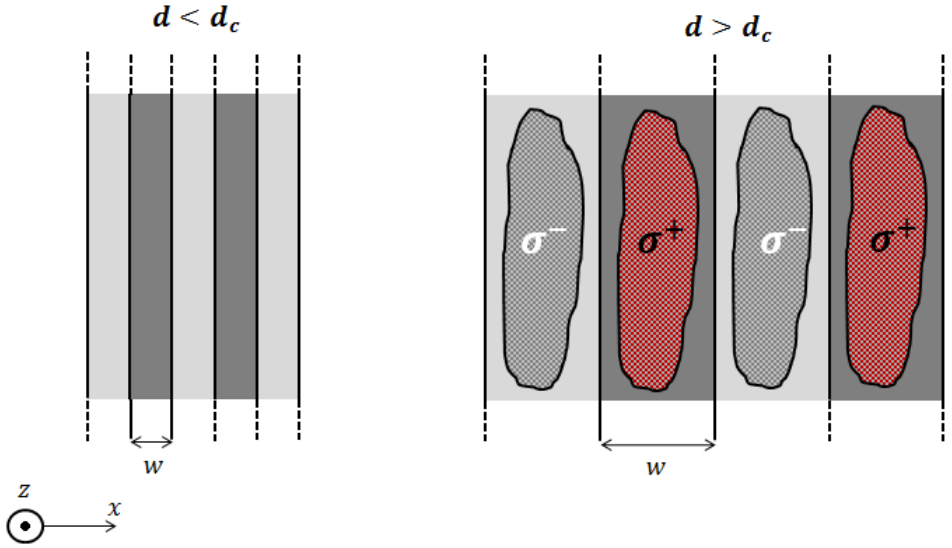

Figure 6: **Left picture** shows the ferroelectric film in the 180° polydomain state, each colored box representing a domain of opposite polarization perpendicular to the OXY plane. No 2DEG has formed yet since film thickness is below critical thickness. **Right picture** shows the system in the coexistence region with $d > d_c$

3 2DEG and Ferroelectric Domain Coexistence: A Model

The model presented in this thesis aims to connect the two seemingly mutually exclusive polarity compensation mechanisms, ferroelectric domains and 2DEG, by joining two different models: the aforementioned model accounting for the formation of a 2DEG in ferroelectrics [5] and the Kittel-Mitsui-Furuichi theory and electrostatics of ferroelectric domains [18, 19, 25] in ferroelectric thin films.

3.1 Formation of 2DEG at ferroelectric interfaces

The formation of the 2DEG at ferroelectric interfaces is approached through a phenomenological model originally presented in Ref.[5] in which only the transition from paraelectric phase to ferroelectric monodomain phase with a 2DEG is taken into consideration. The model will encompass several energetic contributions and the free energy per unit volume for the ferroelectric thin film of thickness d can be formulated as follows[4]:

$$G_G = U_0 + \frac{\sigma\Delta}{d} + \frac{\sigma^2}{2gd} + \frac{1}{2\varepsilon_0}(\sigma - P)^2 \tag{3.1}$$

The first term, U_0 is the free energy of the bulk ferroelectric at zero field. The second and the third terms account for the energy needed for carriers to make an interband transition from top of the valence band at the surface of the ferroelectric to the bottom of the conduction band at the interface – the process described by the *electronic reconstruction* as a result of the *polar catastrophe*. The last term is the electrostatic energy due to the depolarizing field in the ferroelectric monodomain phase.

To express the free energy of the bulk ferroelectric at zero field U_0, Landau theory (LT) for phase transitions is employed. Landau theory is the analysis of the equilibrium behaviour of the system near a phase transition based solely in symmetry considerations. The phase transition is characterized in terms of an *order parameter*, which must be zero above the critical temperature for the high-symmetry disordered phase – paraelectric phase in the context of ferroelectrics – and must continuously change to a finite value when the symmetry is lowered – ferroelectric polarized phase in perovskites.

[4]The subscript «G »in G_G stands for «Gas ».

The order parameter chosen to account for the paraelectric-to-ferroelectric phase transition in ABO_3 perovskites, the foundation materials of our analysis, will describe the distortion of the unit cell during the transition: the oxygen cage displacement with respect to the cations. However, since this soft mode marks the transtion to a polar configuration, it will be natural to take the polarization density associated with the mode as the order parameter,

$$P_\eta = \frac{1}{\Omega} Z_\eta^* \eta \tag{3.2}$$

Ω being the unit-cell volume and Z_η^* being the effective charge associated with the soft mode. The Landau expansion of the bulk ferroelectric free energy per unit volume in terms of the order parameter will have a *double-well* shape from which the phenomenology – different equilibrium configurations – described by (3.1) is derived,

$$U_0 = \frac{A}{2}(T - T_c)P_\eta^2 + \frac{B}{4}P_\eta^4 + O(P_\eta^6) \tag{3.3}$$

However, the total polarization P of the material must take into account the arbitrary electrostatic boundary conditions. Therefore, the total polarization will be the sum of the polarization originated in the distortive phase transition, due to the *soft mode* and that due to the presence of a finite electric field[5],

$$P = P_\eta + P_e = P_\eta + \varepsilon_0 \chi_\infty E \tag{3.4}$$

where $\varepsilon_\infty = \chi_\infty + 1$ is the background electronic contribution to the permitivity of the ferroelectric. The Landau expansion for the bulk ferroelectric free energy in arbitrary boundary conditions – where now both the distortive phase transition and background electronic contribution are being taken into account – can finally be expressed as,

$$U = \frac{1}{2\varepsilon_0 \chi_\eta}\left(\frac{1}{4}\frac{P_\eta^4}{P_s^2} - \frac{1}{2}P_\eta^2\right) + \frac{1}{2\varepsilon_0 \chi_\eta}P_e^2 \tag{3.5}$$

The parameters A and B in (3.3) have been substituted by characteristic magnitudes in the material: P_s is the spontaneous polarization of the ferroelectric in absence of the depolarizing field, $\varepsilon_0 \chi_\eta$ constitutes the contribution of the soft mode associated with the phase transition to the polarizability around P_s and the last term takes into account extra polarization due to electrons and other phonons.

[5]Once again, linear dielectric response of the material being assumed.

The model presented in (3.1) is completed by accounting for the energy needed to create free carrier accumulation. The second term in eq. (3.1) refers to the energetic cost (in volume units) of transferring charge across the band gap, which will simply be taken to be the band gap of the bulk ferroelectric. The third term comes into play if a finite density of states is considered and is related to the filling of both valence and conduction bands – valence band with holes and conduction band with electrons. The density of states written in eq. (3.1) is actualy the reduced density of states combining both the density of electron and hole states (g_e and g_h),

$$g = \frac{g_e g_h}{(g_e + g_h)} \tag{3.6}$$

each of which has been taken as a constant, as we would for a two-dimensional system.

By rearrenging the terms in eq. (3.1) and introducing the information contained in eq. (3.5), the model is formulated so that it quantifies the formation of electron-hole pairs separated by the electric field across the ferroelectric film,

$$G_G = \frac{1}{2\varepsilon_0\chi_\eta}\left(\frac{1}{4}\frac{P_\eta^4}{P_s^2} - \frac{1}{2}P_\eta^2\right) + \frac{1}{2\varepsilon_0\varepsilon_\infty}(P_\eta - \sigma)^2 + \frac{\Delta\sigma}{d} + \frac{\sigma^2}{2gd} \tag{3.7}$$

At fixed ferroelectric film thickness d, the parameters in charge of system energy minimization will be σ, the accumulated free surface charge (2DEG) and P_η, the polarization appearing as a consequence of the phase transition. This first model is plotted in figure 4 as the red curve.

3.2 Ferroelectric domains: Kittel-Mitsui-Furuichi electrostatics

Ferroelectric domains represent an alternative stabilizing means for the system to find its equilibrium configuration. This mechanism competes with the formation of the 2DEG since a polydomain configuration may lead to zero net polarization at surface and interfaces, cancelling any chances of electronic reconstruction and formation of the 2DEG taking place.

In order to model the energy of a ferroelectric thin film broken into domains we will again assume a 180° domain pattern as previously shown in figure 3. The energy

per unit volume of the system will be the sum of the bulk ferroelectric free energy already presented in the previous section eq. (3.3), the energy cost of creating domain walls (2.11) and the electrostatic energy associated to the depolarizing field in the periodic pattern (2.9). Thus, the energy density in the Kittel-Mutsui-Furuichi theory is[6]:

$$G_D = U_0(P_S) + \frac{\Sigma}{w} + U_{dep} \tag{3.8}$$

where the only variable determining the configuration of the system at fixed film thickness d is the domain pattern period w for P_η has been taken as P_S, the ferroelectric phase well established.

3.3 A model for the coexistence: The α model

Coexistence of the 2DEG and ferroelectric domains will be explored through a Landau theory based phenomenological model that merges both mutually exclusive limits introduced in previous sections: eq. (3.7) and eq. (3.8),

$$G = G(P_\eta, \sigma, w) \longrightarrow G_G \cup G_D. \tag{3.9}$$

The model, which will be referenced as the α-model, will combine each of the distinct contributions to the energy of the system discussed in the two previous sections. The parameters for its minimization at fixed film thickness will be the polarization P_η related to the soft mode η, free surface charge σ linked to the 2DEG and ferroelectric domain width w. The energy function 3.9 will incorporate the bulk ferroelectric free energy per unit volume,

$$U_0(P_\eta) = \frac{1}{2\varepsilon_0\chi_\eta}\left(\frac{1}{4}\frac{P_\eta^4}{P_s^2} - \frac{1}{2}P_\eta^2\right) \tag{3.10}$$

the energy cost for promoting electrons across the band gap and filling the bands with finite density of states,

$$U_{2DEG}(\sigma) = \frac{\Delta\sigma}{d} + \frac{\sigma^2}{2gd} \tag{3.11}$$

and the contribution from domain wall energy,

$$U_W(w) = \frac{\Sigma}{w} \tag{3.12}$$

[6]The subscript «D»in G_D stands for «Domain».

In addition to these separate contributions, there is one term left to be added to the energy cost function: the electrostatic energy of the system. Formulation of this term, however, is not as straightforward as the rest of the individual contributions in the model. Each of these former contributions belongs to either the theory of the formation of the 2DEG (3.7) or creation of ferroelectric domains (3.8). They only account for the phenomenon they describe and for which they have been introduced: either the free bulk energy, the formation of domain walls or promotion of carriers across bands.

Therefore, each of them is simply added as a separate contribution to the energy G in (3.9). Nevertheless, the electrostatic energy term in the α-model must take into account the whole picture (as its schematic representation shows in figures 5 and 6), the full equilibrium state of the system, and must reflect both the existence of the 180° domain pattern as well as the 2DEG at the surface or interface of the film.

The electrostatic energy term we are looking for must link two limits. On the one hand, the electrostatics of a capacitor where its surface charge is partially screened by the accomulation of free carriers, the 2DEG – this would be the analog of the system we are dealing with in the monodomain phase limit, $x = d/w \ll 1$. On the other hand, KMF electrostatics, where the electrostatic energy must diverge with decreasing the film thickness and domain width w follows the KMF square root law (2.3).

The electrostatic energy expression given in (2.9) can be modified to meet both the capacitor limit and KMF electrostatics by simply considering that the formation of the 2DEG would screen the spontaneous polarization reducing its value. Since the expression was computed for a ferroelectric system broken into domains, it already reproduces the KMF square root law by construction. The effect of the electron gas is introduced by sustracting σ to the polarization of the ferroelectric film. The convergent series could thus be rewritten as:

$$U_{\text{elec}}^{(\text{dep})} = \frac{8(P-\sigma)^2}{\pi^3 \varepsilon_0} \frac{w}{d} \sum_{n=1}^{\infty} \frac{1}{n^3} \sin^2\left(\frac{n\pi}{2}\right) \frac{1}{1 + \sqrt{\kappa_a \kappa_c} \coth\left(\frac{n\pi}{2} \sqrt{\frac{\kappa_a}{\kappa_c}} \frac{d}{w}\right)} \tag{3.13}$$

In the limit of ferroelectric domain width w much greater than film thickness d ($x = d/w \ll 1$), the series converges towards eq. (2.10), where the surface charge term

has now been substituted by $(P - \sigma)$ to account for the electron gas at the surface[7]. We have caoutiously written P, the total polarization of the system, instead of P_η to account for both the soft-mode polarization and the background electronic contributions, and to cautiously introduce the effect of background permitivity.

Expression (3.13), although rigurously correct in all its complexity, can nevertheless be sustituted by the following, simpler term that will easen the analytical resolution of the α-model and will be tested as a simplifiying substitution for (3.13):

$$U_{\text{elec}}^{(\alpha)} = \frac{(P_\eta - \sigma)^2}{2\varepsilon_0}\left[\varepsilon_\infty^\alpha + \left(\frac{d}{\beta w}\right)^\alpha\right]^{-1/\alpha} \tag{3.14}$$

where ε_∞ is the background permitivity and β takes the form:

$$\beta = \frac{2 \times 8.416}{\pi^3(1 + \sqrt{\kappa_c \kappa_a})} \tag{3.15}$$

The expression contains α as a parameter. It indicates the slope of the function at the origin (when $x = d/w \to 0$) and controls its smoothness. The analysis of the derivative at the origin leads to the conclusion that the slope of the function when $x \to 0$ will take a non-zero value if $\alpha = 1$ and zero if α takes any other value.

Condition $\alpha > 0$ must be satisfied for expression eq. (3.14) to make sense; otherwise, neither the capacitor limit nor Kittel-Mitsui-Furuichi electrostatics would be reproduced. Besides, in the large domain width limit ($x = d/w \ll 1$) very few domain walls are expected, if any. Therefore, a Taylor expansion of eq. (3.14) around the origin will show that α regulates the corrections to the capacitor electrostatic energy 2.10.

Depending on the value of α, this Taylor expansions around $x \to 0$ yield:

$$\lim_{x\to 0} U_{\text{elec}}^{(\alpha)}(x) \sim \frac{(P_\eta - \sigma)^2}{2\varepsilon_0\varepsilon_\infty}\left[1 - \frac{d}{\varepsilon_\infty \beta w}\right] \qquad \text{for } \alpha = 1 \tag{3.16}$$

$$\lim_{x\to 0} U_{\text{elec}}^{(\alpha)}(x) \sim \frac{(P_\eta - \sigma)^2}{2\varepsilon_0\varepsilon_\infty}\left[1 - \left(\frac{d}{\varepsilon_\infty \beta w}\right)^2\right] \qquad \text{for } \alpha = 2 \tag{3.17}$$

[7] The electron gas forming at the surface or heterointerface of the system when the monodomain phase is stable will depend on the direction of the depolarizing field it has to counteract.

The correction to the capacitor electrostatic energy in each of the expressions will have different physical interpretations. The correction for $\alpha = 1$ suggests that the electrostatic energy is lowered at the origin due to the remaining domain walls. The correction for $\alpha = 2$ surprisingly suggests that the scarce domain walls yet coexisting do see and weakly interact with each other. Higher values of α lead to smaller corrections which were not considered to give further physical insight. Moreover, computations made for higher values of α (3, 4, 5...) showed eq. (3.14) was no longer comparable to the expression found in literature, eq. (3.13), and disagreement between these functions lead to consider $\alpha = 1$ and $\alpha = 2$ only.

Figures 7 and 8 show a comparison between the most general electrostatic expression (3.13), the simplifying electrostatic term built for the α model (3.14) (for $\alpha = 1$ and $\alpha = 2$) and its limit when KMF electrostatics dominate ($x = d/w \gg 1$),

$$U_{\text{elec}}^{(\text{KMF})} = \frac{(P_\eta - \sigma)^2}{2\varepsilon_0}\beta\frac{w}{d} \tag{3.18}$$

Both plots show that the proposed electrostatic term, $U_{\text{elec}}^{(\alpha)}$, correctly goes towards the Kittel limit and the main disagreement between eq. (3.13) and eq. (3.14) is obtained in the monodomain region ($x = d/w \to 0$), where the electrostatic term in the α model behaves differently depending on the value α itself takes. Function (3.13) has a non-zero slope at the origin, suggesting the correct value for α is 1. However, eq. (3.14) most correctly reproduces (3.13) if α is taken as 2. Discussion on which value of α to choose will be followed in subsequent sections. In order to obtain the plots in figures 7 and 8, P_η was again assumed to take its saturation value P_S.

The full model subjected to analysis in this thesis is finally presented,

$$G = \frac{1}{2\varepsilon_0\chi_\eta}\left(\frac{1}{4}\frac{P_\eta^4}{P_s^2} - \frac{1}{2}P_\eta^2\right) + \frac{\sigma\Delta}{d} + \frac{\sigma^2}{2gd} + \frac{\Sigma}{w} + \frac{(P_\eta - \sigma)^2}{2\varepsilon_0}\left[\varepsilon_\infty^\alpha + \left(\frac{d}{\beta w}\right)^\alpha\right]^{-1/\alpha} \tag{3.19}$$

Expression (3.19) will be used to find the equilibrium surface/interface charge σ as well as domain width w in the ferroelectric thin film. Coexistence of ferroelectric domains and 2DEG will be proved if a smooth transition between the polydomain configuration (finite w) and monodomain configuration (divergent w) is observed while σ being nonzero, in opposition to the sharp transition predicted by published works [5, 6]. It is important to remark that a finite density of states (DOS) g must be considered, since the coexistence will critically depend on it.

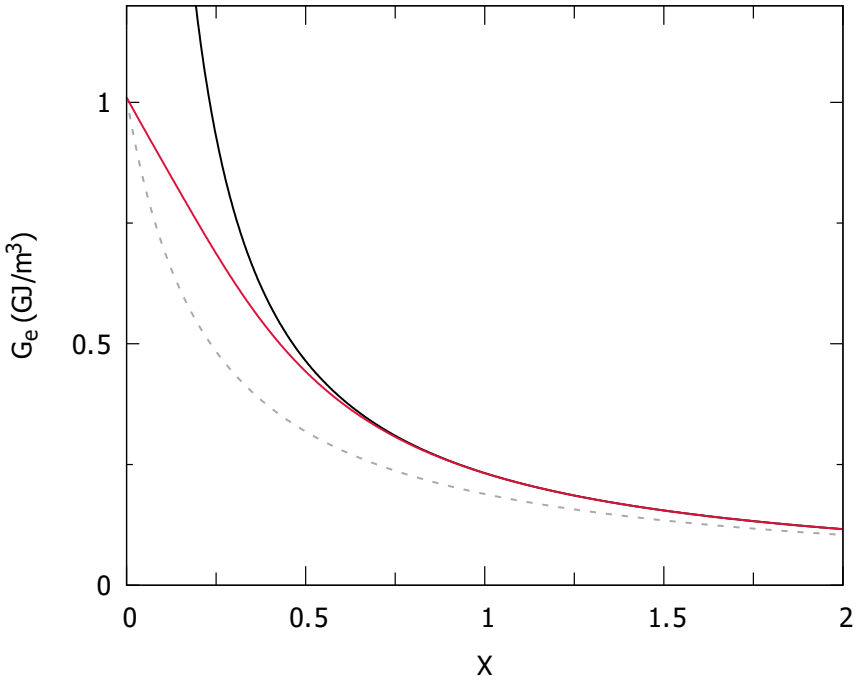

Figure 7: Comparison of the electrostatic energy term due to the depolarazing field for a 180° domain pattern plotted against x (d/w). **In red**, expression given by eq. (3.13), the **dashed line** corresponds to the electrostatic energy term in the α model **($\alpha = 1$)** and the **black solid** line is the electrostatic energy in the Kittel limit.

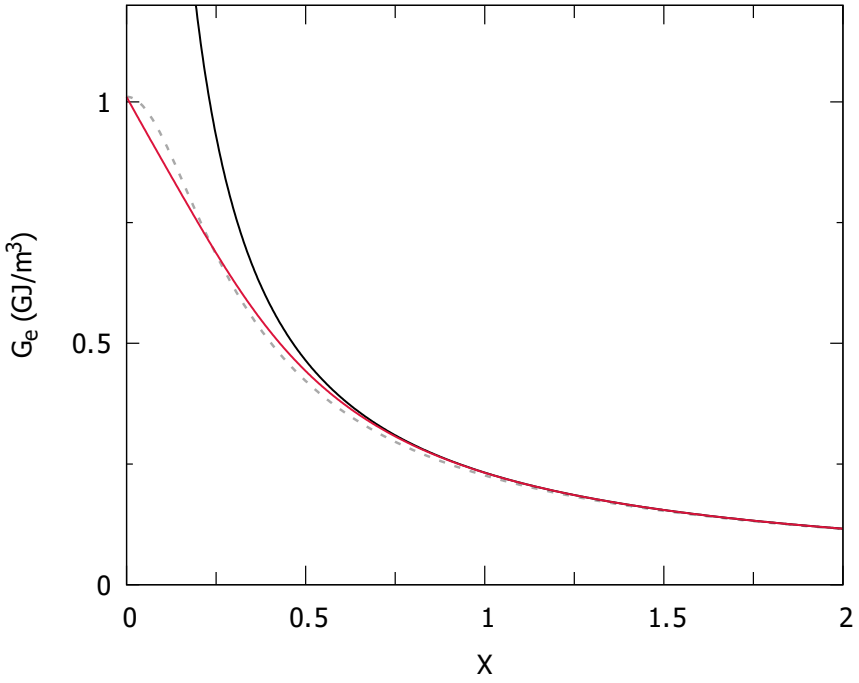

Figure 8: Comparison of the electrostatic energy term due to the depolarazing field for a 180° domain pattern plotted against x (d/w) as in figure 7. The dashed line corresponds now to the α model with $\alpha = 2$.

4 Model Resolution

In order to solve the model presented in eq. (3.19), parameters characterizing the equilibrium configuration of the system (P_η, w and σ) must be found and physical interpretation to the outcome be given. Therefore, the procedure to be followed is clear: we must solve a global optimization problem. Finding the global minimum for the α-model will be attempted from both analytical and numerical approaches.

4.1 Analytical Resolution: An approximation

The α-model can be analytically solved as long as certain approximations are made. These simplifications are listed below:

a) The polarization P_η will be assumed to take its saturation value P_s, indicating that the system is far from the region where the phase transition takes place and the ferroelectric phase is well stabilized.
b) Film thickness d will be taken larger than domain width ($x = d/w \gg 1$), so that the analytical resolution is performed for values of d where the Kittel-Mitsui-Furuichi part ($U_{\text{elec}}^{(\text{KMF})}$) is dominant and thus becomes the electrostatic contribution.

Under these considerations, the model simplifies to

$$G(w,\sigma) = U_0(P_s) + \frac{\sigma\Delta}{d} + \frac{\sigma^2}{2gd} + \frac{\Sigma}{w} + \frac{(P_s-\sigma)^2}{2\varepsilon_0}\beta\frac{w}{d} \tag{4.1}$$

where the ambiguity in what value to choose for α dissapears due to the second condition (b) listed above. For fixed ferroelectric film thickness, the equilibrium configuration of the system can be obtained by minimizing eq. (4.1) with respect to its variables, w and σ,

$$\frac{\partial G}{\partial w} = 0 \qquad \text{and} \qquad \frac{\partial G}{\partial \sigma} = 0 \tag{4.2}$$

which yield a system of two coupled algebraic equations. Algebraic manipulation leads to the explicit formula to compute equilibrium carrier density, given by the expression,

$$\sigma = g\Big(\sqrt{\frac{2\beta\Sigma d}{\varepsilon_0}} - \Delta\Big) \tag{4.3}$$

Under the constraint that $\sigma \geq 0$, a critical thickness below which free carriers forming the 2DEG are unable to perfom an interband transition can be computed. The electronic reconstruction process will only take place once the film has reached a thickness exceeding the critical value,

$$d_c = \frac{\varepsilon_0 \Delta^2}{2\beta\Sigma} \tag{4.4}$$

The KMF law (as expressed in eq. (2.3)) can explicitly be formulated as:

$$w^2 = \frac{\Sigma}{\gamma} d \quad \text{where} \quad \gamma = \frac{P_s^2}{2\varepsilon_0}\beta \tag{4.5}$$

The length value at which the ferroelectric domain width w equals film thickness ($w = d$) is called *Kittel's length*, $l_k = \Sigma/\gamma$. This parameter will help us check the range of validity of the analytical solutions obtained from the simplifications made to the model. Solutions are expected to be valid when $d \gg w$; that is, the behaviour depicted by the curves obtained (figure 9) will only provide us with physically acceptable solutions when they are below the function $w = d$.

Minimization of eq. (4.1) finally leads to

$$\sigma = g\Delta\Big(\sqrt{\frac{d}{d_c}} - 1\Big) \tag{4.6}$$

$$w = \frac{\sqrt{l_k d}}{\Big[1 - \frac{g\Delta}{P_s}\Big(\sqrt{\frac{d}{d_c}} - 1\Big)\Big]} \tag{4.7}$$

As eq. (4.7) establishes, domain width w no longer follows the classical KMF square root law. In contrast, domain width does grow with increasing film thickness but its dependence with d is more complex than that predicted by the KMF law. The value at which w diverges will be labelled as d_p,

$$d_p = d_c\Big(\frac{P_s}{g\Delta} + 1\Big)^2 \tag{4.8}$$

The divergence of domain width w must be physically interpreted as the stabilisation of the system in the monodomain phase, where the domain pattern period goes to infinity ($w \to \infty$).

Free surface carrier density σ will be zero below critical thickness d_c and will grow proportional to the square root of the film thickness above d_c until it manages to screen the spontenous polarization P_S in the ferroelectric film, the screening of P_S indeed being very effective. Once the system has become stable and the sponteous polarization is screened, σ saturates, indicating that the accumulation of surface charge has stopped. This saturation takes place once the monodomain phase is stable at d_p. The behaviour of σ can thus be summarized by,

$$\sigma = \begin{cases} P_S & \text{if } d \geq d_p \\ g\Delta\left(\sqrt{\frac{d}{d_c}} - 1\right) & \text{if } d_c < d < d_p \\ 0 & \text{if } d \leq d_c \end{cases} \tag{4.9}$$

Analytical functions given by eq. (4.9) and eq. (4.7) have been depicted in figure 9. The behaviour shown there is valid for $x = d/w \gg 1$. The maximum validity thickness d_v will indicate that above it, the outcome obtained from the aproximated version of the α-model is no longer credible.

When eq. (4.7) exceeds the function given by the condition to compute l_k ($w = d$), the analytical resolution ceases to be reliable. The thickness d_v is thus defined by the trascendent equation,

$$d_v^2\left[1 - \frac{g\Delta}{P}\left(\sqrt{\frac{d_v}{d_c}} - 1\right)\right]^2 = l_k d_v \tag{4.10}$$

Nevetheless, since typical Kittel lengths l_k are about an order of magnitude smaller compared to the expecting values for the diverging limit d_v (characteristic lenght for PTO is ~ 0.11nm [20]), it can be estimated that d_v is indeed a value around d_p: the trascendent equation yields the same condition for the divergence of w used to compute d_p,

$$\left[1 - \frac{g\Delta}{P}\left(\sqrt{\frac{d_v}{d_c}} - 1\right)\right] = \sqrt{\frac{l_k}{d_v}} \approx 0 \tag{4.11}$$

This proves the approximation is valid in almost all range of interest, the coexistence region, and will break for both thin film limit and thick film limit.

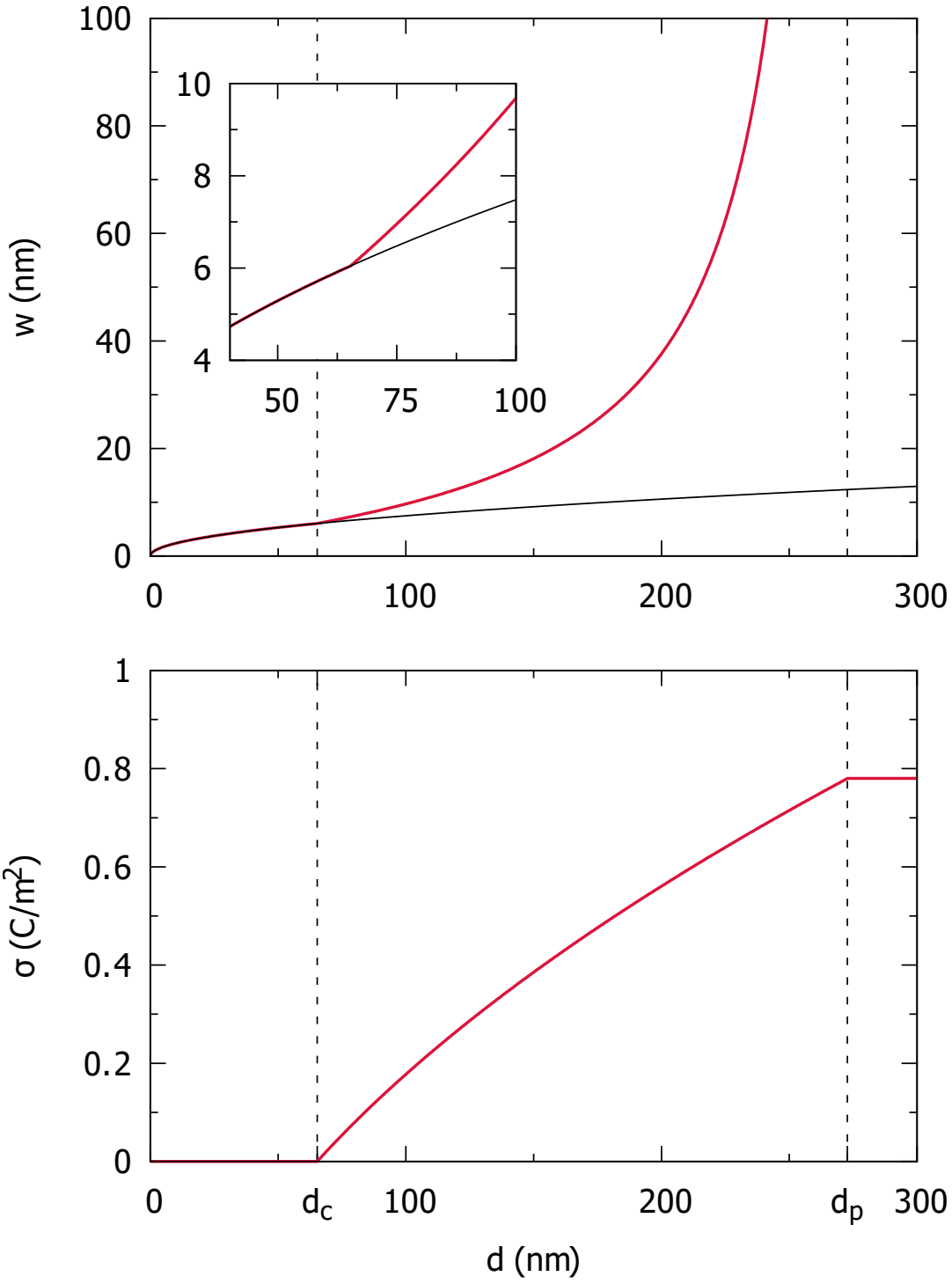

Figure 9: **Upper panel**: In red, ferroelectric domain width plotted against film thickness for the analytical resolution of the model. Dashed line corresponds to KMF law. *Inset plot*: Critical thickness at which the 2DEG begins to form. For a band gap of $e\Delta = 3.6$ eV, $d_c \sim 65$ nm. **Lower panel**: Evolution of surface charge density (2DEG) with film thickness. The electron gas is non-existent up to the critical thickness and then grows until it saturates, coincident with the spontaneous ferroelectric polarisation which intends to screen.

4.2 Numerical Resolution

We resort to optimization algorithms in order to obtain numerical resolution of the full coexistence model (3.19) without making any approximations as those required by the analytical resolution in the previous section.

Discussion in section 3.3 revealed the difficulty in choosing the correct electrostatic term accounting for both screening mechanisms – 2DEG and ferroelectric domains. The α-containing electrostatic term, $U_{\text{elec}}^{(\alpha)}$, served as a simplification of the general formulation shown in eq. (3.13). However, the simplified electrostatic term required α itself to be determined. As both $\alpha = 1$ and $\alpha = 2$ are reasonable choices, numerical computations were carried out considering the model with three different electrostatic terms: equation (3.13) and equation (3.14) with $\alpha = 1$ and $\alpha = 2$, being these values of α the ones allowing for the best recreation of eq. (3.13).

Numerical computations were performed by using the *Scipy* Open Source Scientific Library [21]. Two different approaches were tested: *root-finding* methods to solve the system of coupled algebraic equations obtained when the function $G = G(P_\eta, \sigma, w)$ is differentiated with respect to its variables,

$$\partial_{P_\eta} G = 0 \qquad \partial_\sigma G = 0 \qquad \partial_w G = 0 \tag{4.12}$$

and *global optimization* methods, where finding the global minimum of $G = G(P_\eta, \sigma, w)$ is directly attempted.

None of the root-finding algorithms tested turned out to be satisfactory. When turning to brute force global optimization methods – those scaning the whole solution space – it was found the methods were unable to find the global minimum because, although the position of this minimum changed with growing film thickness, it was located in a flat valley. The algorithms would at first converge to spurious solutions.

Therefore, contour plots of the model G as a function of P_η and w were made for different thicknesses to delimit the location of the minimum. In order to do so, the number of variables of the cost function G was reduced by introducing the σ that would minimize the α-model as solved for σ in (4.12). Then, instead of allowing the algorithms to work by brute force, their search was restricted to regions of the solution

space were solutions were expected to be found. This information was passed to the algorithm employed, making it easier for it to find the correct solution.

4.2.1 Differential Evolution: An Algorithm for Global Optimization

Numerical solutions shown in this work were obtained by Differential Evolution, the algorithm used as the numerical solver for the α-model without any approximations being made. The algorithm due to Rainer Storn and Kenneth Price [22] is part of the so-called *evolutionary computation*, a group of global optimization methods inspired by the theory of biological evolution: the population – vectors in the solution space – is subjected to selection and mutation processes to gradually increase its fitness to the cost function, the function to be minimized 3.19.

The algorithm consists of three phases that run iteratively improving the candidate solution in each generation: *mutation, crossover* and *selection*. The first initiallized generation G consists of D-dimensional NP $\vec{x}$ target vectors which can either be randomly chosen or introduced as a preliminary guess.

If the algorithm is first run for the thin film limit ($d \ll d_c$), a clever preliminary choice as the initial guess is to entail variables to stick to KMF law (4.5). In the coexistence α-model (3.19), the dimension of each candidate vector belonging to a particular generation is $D = 3$, the components of which are the variables P_η, σ and w. As suggested by Storn and Price [26], the dimension of each population – the *number of parents*, NP – was chosen to be ten times the dimension of each vector.

Once the initial target generation is either conviniently or randomnly chosen, the mutation phase takes place. During this phase, new candidate vectors $\vec{v}$ are created as a combination of randomly chosen target vectors,

$$\vec{v}_{i,G+1} = \vec{x}_{r1,G} + F \times (\vec{x}_{r2,G} - \vec{x}_{r3,G}) \qquad F \in [0,2] \tag{4.13}$$

where the subscript r stands for *random*. The weighting factor F controls the amplification of the differential variation between target vectors from the former generation and this way, the mutant generation vectors $\vec{v}_{i,G+1}$ are born.

The crossover phase is then run to increase diversity among candidate solutions by creating a new trial vector generation. This is obtained by mixing the components from vectors in the initial target generation and vectors from the mutant generation,

$$(u_{mn})_{i,G+1} = \begin{cases} (v_{mn})_{i,G+1}, & \text{if } k \leq CR \\ (x_{mn})_{i,G}, & \text{if } k > CR \end{cases} \tag{4.14}$$

where k is a random number such that $k \in [0, 1]$. CR is the crossover constant and is also constrained to take values between 0 and 1.

Finally, the selection process consists of determining which of the vectors in the former generations (*target* or *crossed* generation) provides a better fitting to the cost function (3.19) and therefore, should become a member of the following generation. In order to do so, the *greedy criterion* is used. If a trial generation vector, $\vec{u}_{i,G+1}$, is selected as a better candidate in comparison to the target generation vector $\vec{x}_{i,G}$, leading to a smaller cost function value, it will become part of the new target generation; otherwise, $\vec{x}_{i,G}$ is kept. As it is usual for iterative methods, the algorithm will be running until convergence is achieved; that is, until the computed difference of two solution for the minimum of G is below a certain threshold.

Convergence and physically acceptable solutions for the cost function given by eq. (3.19) were obtained by taking the DE parameters as

$$F = 0.2 \qquad CR = 0.9 \qquad NP = 30. \tag{4.15}$$

The algorithm required to know the bound values of each of the variables. It was found that working with the inverse of ferroelectric domain width $k = 1/w$ (which might as well be understood as ferroelectric domain frecquency) led to convergency faster than w itself as the variable. This is because in the monodomain limit ($x = d/w \ll 1$), when w is expected to diverge, its inverse k will go to zero. Therefore, the transition to the monodomain limit and the thickness at which it becomes stable are clearly visible.

Solutions provided by the DE algorithm were also required to simultaneously satisfy a threshold settled by the three non-linear algebraic equations derived from (3.19) that minimize G,

$$\frac{1}{2\varepsilon_0\chi_\eta}\left(\frac{P_\eta^3}{P_s^2}-P_\eta\right)=\frac{(\sigma-P_\eta)}{\varepsilon_0}\left[\varepsilon_\infty^\alpha+\left(\frac{d}{\beta w}\right)^\alpha\right]^{-1/\alpha} \tag{4.16}$$

$$\frac{\Delta}{d}+\frac{\sigma}{gd}=\frac{(P_\eta-\sigma)}{2\varepsilon_0}\left[\varepsilon_\infty^\alpha+\left(\frac{d}{\beta w}\right)^\alpha\right]^{-1/\alpha} \tag{4.17}$$

$$\frac{\Sigma}{w^2}=\frac{(P_\eta-\sigma)^2}{2\varepsilon_0}\left[\varepsilon_\infty^\alpha+\left(\frac{d}{\beta w}\right)^\alpha\right]^{-(1+\alpha)/\alpha}\left(\frac{d}{\beta w}\right)^\alpha\frac{1}{w} \tag{4.18}$$

There is a subtlety to be taken into consideration when asking the solutions to satisfy the threshold settled by the three equations above, and that is that equation (4.17) will not make sense for $d < d_c$ since the 2DEG has not formed yet and thus $\sigma = 0$. This equation must only be established as a condition to be satisfied when $d \geq d_c$.

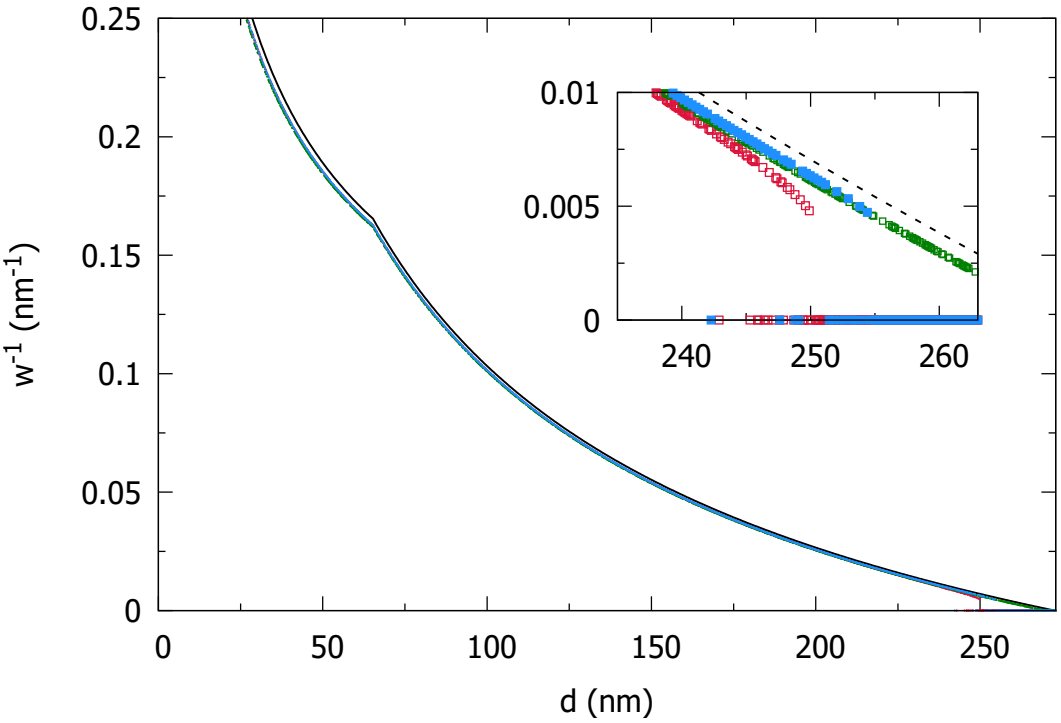

Figure 10: Inverse of domain width w plotted against film thickness. ***Inset plot***: Region were w diverges and from which values of d_p are computed.

As stated before, the coexistence of both screening mechanisms will critically depend on the finite density of states. If $g \to \infty$ had been considered as a plausible approximation, neither the analytical resolution for σ and w – equations 4.6 and 4.7 – nor the numerical resolution would be showing a coexistence region between d_c and d_p. Instead, σ would have been pinned from the beginning, independent of thickness d, an outcome that contradicts the theory exposing the existence of a critical thickness d_c.

4.3 Case Study: the PTO/STO system

Practical application of the optimization algorithm was made for a prototypical ferroelectric material: a ferroelectric thin film of lead titanate ($PbTiO_3$) embedded over a strontium titanate ($SrTiO_3$) perovskite substrate as schematically shown in figure 5 – the PTO/STO system. $PbTiO_3$ is a ferroelectric perovskite-type compound with high Curie temperature ($\sim 500°C$) and a fairly high tetragonal distortion, where P_η will almost always take its P_S saturation value. This was confirmed by the numerical resolution. Material parameters for the system were taken from [5], where authors obtained them from first principle calculations,

P_S (C/m^2)	Σ (mJ/m^2)	χ_η	κ_c	κ_a	ε_∞	g_e/e^2 ($m^{-2}J^{-1}$)	g_h/e^2 ($m^{-2}J^{-1}$)
0.78	0.13	26	35	185	7	1.2×10^{37}	2.5×10^{37}

Table 1: Parameter values used in the numerical resolution, from [5]

As for the film band gap Δ, the experimental value was used, $e\Delta = 3.6$ eV. The numerical outcome is shown in figure 11.

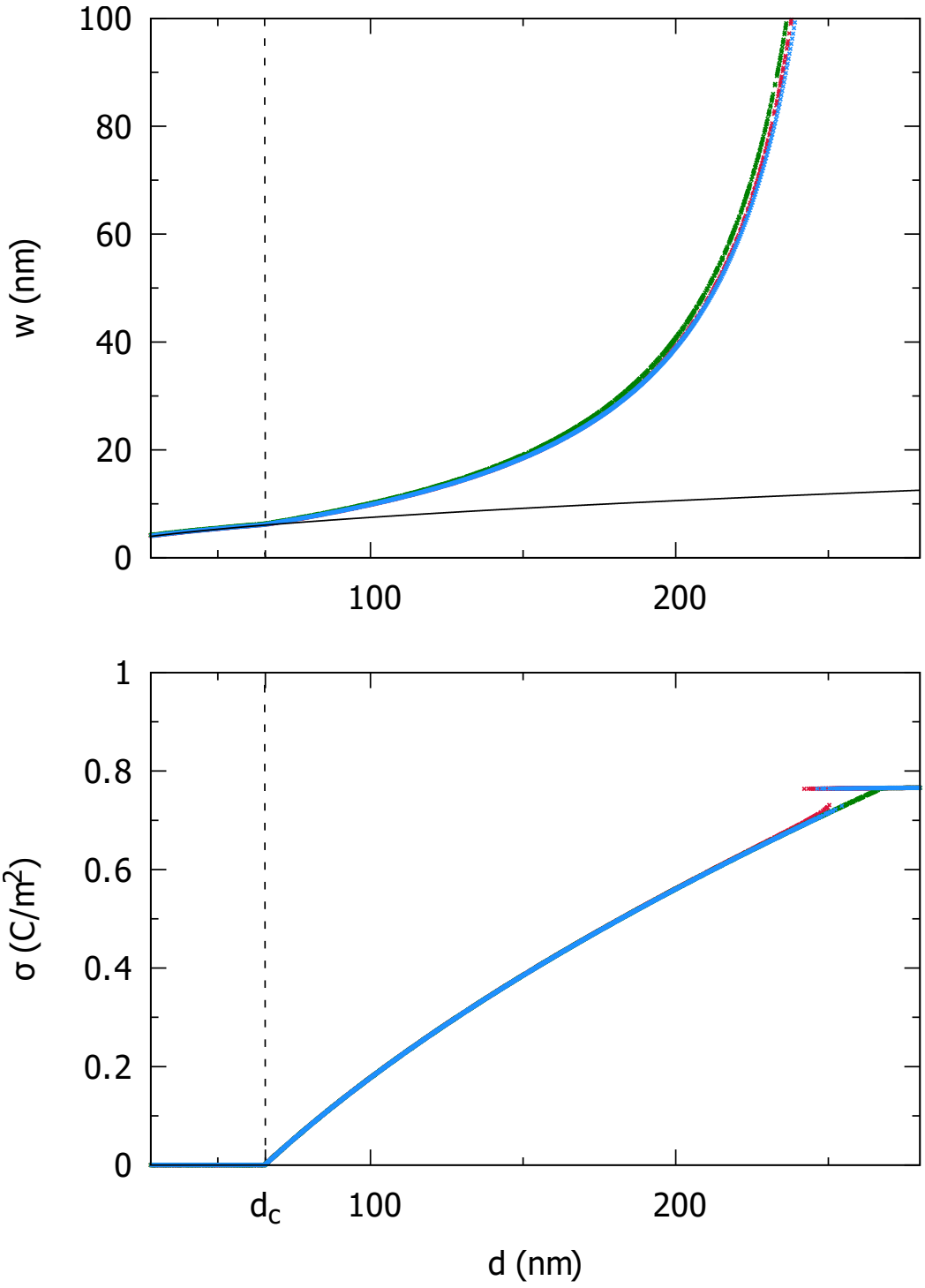

Figure 11: **Upper panel**: Ferroelectric domain width w plotted against film thickness w as given by numerical resolution (PTO/STO case). Blue points correspond to the α-model where $U_{\text{elec}}^{(\text{dep})}$ was used as the electrostatic term. Green points correspond to the α-model with $U_{\text{elec}}^{(\alpha=1)}$ and red points correspond to $U_{\text{elec}}^{(\alpha=2)}$. The black solid line is the KMF law. **Lower panel**: Free surface carrier density σ plotted against film thickness. The thickness d_c marks the formation of the 2DEG. The x-axis is shared by both plots.

5 Discussion

Both numerical and analytical resolution of the α-model (Figures 9 and 11) confirm there is a *smooth transition* between the ferroelectric polydomain state without free surface carriers and the monodomain phase stabilized by means of the formation of a 2DEG. The coexistence region for both competing screening mechanisms is bounded between the critical thickness d_c and the divergence thickness d_p. The range of thickness values where coexistence is theoretically predicted was numerically estimated by computing the values for d_c and d_p in a system consisting of a lead titanate thin film embedded over an insulating substrate of $SrTiO_3$ (PTO/STO system).

As explained in the previous section, numerical resolution of the α-model (3.19) was performed for three different electrostatic terms: expression (3.13) and expression (3.14) with $\alpha = 1$ and $\alpha = 2$. For each of the electrostatic terms modifying the model, the critical thickness d_c remained invariant and coincident with the analytical result.

	Analytical	U_{Dep}	$\alpha = 1$	$\alpha = 2$
d_c (nm)	65.3	65.3	65.3	65.4

Table 2: Different critical thickness d_c values for each electrostatic term tested.

The numerical resolution of the model was expected to be coincident with the analytical approximated resolution in the neighbourhood of the critical thickness d_c, since this region was within the range of validity of the latter. In fact, the approximations made in section 3.1 erased the need to determine the values taken by α simplifying the electrostatic term in the α-model. Therefore, the difference between each of the G cost functions, depending on the electrostatic term used, is minute in the region where the 2DEG begins to form and hence the resemblance in d_c values shown in table 2.

The period of the 180° stripe domain structure will monotonically increase while obeying the classical Kittel-Mitsui-Furuichi square root law (4.5) up until d_c. Above the critical thickness, the law is no longer followed and surface charge accumulation begins. The formation of the 2DEG is therefore marked by the separation of w from the classical prediction ($w \propto \sqrt{d}$), having larger ferroelectric domains as film thickness grows. Domain width w will then continue increasing until it diverges.

Disagreement between the cost functions employed is revealed in the monodomain limit, where dissimilar values of the divergency thickness d_p are obtained. As shown in figure 4.2.1, the analytical prediction of d_p exceeds the values numerically obtained. However, as argued in section 4.1, the validity of the analytical approximation was restricted by d_v, a thickness value close to d_p which marks the limit in which ferroelectric domain width w is no longer below the function $w = d$. Discrepancy between the analytical and numerical resolution was therefore expected in the monodomain limit, where the analytical resolution might show non-credible behaviour. The analytical outcome is indeed stating that it takes thicker ferroelectric films to achieve a well-stabilized monodomain phase while the numerical solution shows that thinner films do enable the monodomain stable phase.

Values obtained for the divergence thickness d_p depending on the electrostatic term chosen are both listed below and graphically shown for visual comparison,

	Analytical	U_{Dep}	$\alpha = 1$	$\alpha = 2$
d_p (nm)	272.7	252.3	266.1	249.7

Table 3: Different divergence thickness d_p values for each electrostatic term tested.

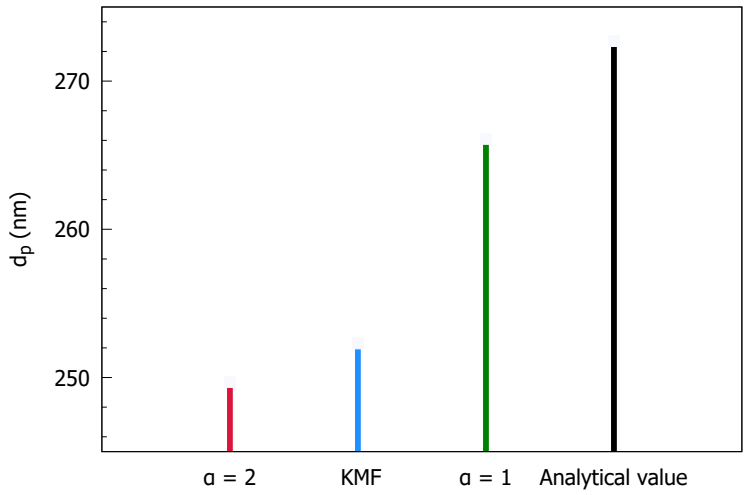

Figure 12: Different values obtained for d_p, depending on the electrostatic term chosen

«Once you have eliminated the impossible, whatever remains, however improbable, must be the truth. »

Sir Arthur Conan Doyle

6 Conclusions

We have used a simple phenomenological Landau-type model to show the coexistence of the two-dimensional electron gas (2DEG) and ferroelectric domains in a ferroelectric thin film as stabilization mechanisms for the equilibrium configuration of the system.

The α-model, name given to the model accounting for the coexistence, has been built as a combination of two different models: one demonstrating that it is possible to stabilize a monodomain phase with an out-of-plane polarization in a ferroelectric thin film over an insulating substrate via 2DEG formation taken from [5] and a second one exposing the energetic cost of ferroelectric domain creation in 180° pattern structure. Both former models regard each screening mechanism as mutually exclusive and predict sharp transitions from the polydomain regime to the monodomain one.

The model accounting for the coexistence of the two screening mechanisms has been both analytically (under certain approximations) and numerically solved. In contrast to published research [5, 6], a *smooth transition* from the ferroelectric polydomain regime to the monodomain phase has been found.

Resolutions place the coexistence region between the critical thickness d_c – as theoretically requested by the electronic reconstruction phenomenon to kick start formation of the electron gas – and the divergence thickness d_p – where the monodomain phase is fully stabilized, domain width w has diverged and consequently, no ferroelectric domains can be found. As a consequence, it is shown that the classical KMF law is no longer satisfied when the formation of the 2DEG begins.

6.1 Future Work

Ongoing technological advances to control thin film growth on the atomic scale enable the fabrication of high-quality oxide interfaces and oxide mutilayers, which constitute sufficiently strong motivation to research further in order to both experimentally confirm the coexistence of the 2DEG and ferroelectric domains in thin films and to extend the coexistence hypothesis to more complex systems. Besides improving the coexistence α-model itself by incorporating new experimental subtleties, adapting the proposed theoretical model from a ferroelectric PTO thin film to a PTO/STO supperlattice system can then be regarded as the next step in research: to explore whether coexistence is feasible in such systems.

Previous works [13] show that insulator to metal transitions can take place at interfaces in LAO/STO oxide superlattice systems with increasing layer thickness. If we were to include ferroelectricity in a superlattice PTO/STO structure, the existence of the depolarizing field would not solely be constrained to the PTO layers but it would also appear in the STO layers. STO will present a spontaneous polarization due to the strain conditions imposed by the geometry formed when creating such multilayered configuration. The α-model should then accordingly be modified to account for the screening of the field via the formation of the 2DEG and ferroelectric domains as well as the screening necessary to stabilize the STO layers. In addition to this, modification of eq. (3.13) should also be made to reflect the new geometry.

As the previous paragraph suggests, because of the many exciting novel phenomena awaiting to be explored, the analysis of the 2DEG formation and the various ways to manipulate it as well as the coexistence of the various system-stabilization mechanisms and the structures they give rise to represent a developing and promising field in both science and technology still in its early stages.

Acknowledgements

I would like to thank Emilio Artacho for his help and support throughout both my internship at CIC nanoGUNE last summer and these months as well as Pablo Aguado for his guidance and availability.

References

[1] A. Ohtomo and H. Y. Hwang, *A high-mobility electron gas at the $LaAlO_3/SrTiO_3$ heterointerface*, *Nature* **vol 427** (2004)

[2] R. Pentcheva, W. E. Pickett, *Electronic phenomena at complex oxide interfaces: insights from first principles*, J. Phys.: Condensed Matter (2010)

[3] N. C. Bristowe, P. Ghosez, P. B. Littlewood and E. Artacho, *The origin of two-dimensional gases at oxide interfaces: insights from theory*, J. Phys: Condens. Matter **26** (2014) 143201

[4] H. Chen, A. M. Kolpak, S. Ismail-Beigi, *Electornic and magnetic properties of $SrTiO_3/LaAlO_3$ interfaces from first principles*, Advanced Materials **vol 22**, Issue 26-27 (2010)

[5] P. Aguado-Puente, N. C. Bristowe, B. Yin, R. Shirasawa, P. Ghosez, P. B. Littlewood and E. Artacho, *Model of two-dimensional electron gas formation at ferroelectric interfaces*, Phys. Rev. B **vol 92** 035438 (2015)

[6] B. Yin, P. Aguado-Puente, S. Qu, E. Artacho, *Two-dimensional electron gas at the $PbTiO_3/SrTiO_3$ interface: an ab initio study*, Phys. Rev. B **92** 115406 (2015)

[7] A. S. Bhalla, R. Guo, R. Roy, *The perovskite structure - a review of its role in ceramic science and technology*, Mat. Res. Innovat (2000) 4:3-26

[8] N. Reyren et al, *Superconducting interfaces between insulating oxides*, Science **317**, 1196 (2007)

[9] S. Thiel, G. Hammerl, A. Schmehl, C. W. Scheneider, J. Mannhart, *Tunable Quasi-Two-Dimensional electron Gases in Oxide Heterostructures*, Science **vol. 313** Issue 5795 (2006)

[10] M. A. Green, A Ho-Baillie, H. J. Snaith, *The emergence of perovskite solar cells*, Nature Photonics **8**, 506-514 (2014)

[11] A. Ohtomo, D. A. Muller, J. L. Grazul and H. Y. Hwang, *Artificial charge-modulation in atomic-scale perovskite titane superlattices*, Nature **419** (2002)

[12] D. G. Schlom, J. Mannhart, *Interface takes charge of Si*, Nature Materials **vol 10**, (2011)

[13] N. C. Bristowe, E. Artacho, P. B. Littlewood, *Oxide superlattices with alternating p and n interfaces*, Phys. Rev. B **80**, 045425 (2009)

[14] N. Nakagawa, H. Y. Hwang, D. A. Muller, *Why some interfaces cannot be sharp*, Nature Materials **vol 5** March (2006)

[15] H. D. Megaw, *Origin of Ferroelectricity in Barium Titane and Other Perovskite-Type Crystals*, Acta Cryst. vol 5 739 (1952)

[16] Y. G. Wang, W. L. Zhong, P. L. Zhang, *Surface and size effects on ferroelectric films with domain structures*, Phys. Rev. B **vol 51** 8 1995

[17] L. Landau, E. Lifshits, *On the Theory of the dispersion of magnetic permeability in ferromagnetic bodies*, Phys. Zeitsch. der Sow, **8** ppg. 153-159 (1935)

[18] C. Kittel, *Physical Theory of Ferromagnetic Domains*, Rev. Mod. Phys. , 21:541-83 (1949), Bell Telephone Laboratories, Murray-Hill NJ

[19] T. Mitsui, J. Furuichi, *Domain Structure of Rochelle Salt and KH_2PO_4*, Phys. Rev. 2, **vol. 90** (1953)

[20] I. S. Vorotiahin et al, *Tuning the polar states of ferroelectric films via Surface Charges and Flexoelectricity*, submitted on 1 Apr 2017 to `arxiv.org`

[21] E. Jones , T. Oliphant , P. Peterson et *al.* , SciPy: Open Source Scientific Tools `scipy.org`

[22] R. Storn, K. Price, *Differential Evolution - A simple and Efficient Heuristic for Global Optimization over Continuous Spaces*, Journal of Global Optimization **11** 341-359 (1997)

Literary Works

[23] R. H. Mitchell, *Perovskites: Modern and Ancient*, Thunder Bay, Ontario: Almaz Press 2002 ISBN 0-9689411-0-9

[24] N. W. Ashcroft, N. D. Mermin, *Solid State Physics*, 1976 Brooks/Cole ISBN-13:978-81-315-0052-1-1

[25] A. K. Tagantsev, L. E. Cross, J. Foussek, *Domains in Ferroic crystals and thin films*, Chapter 5, SPRINGER (2010) 026, ISBN 978-1-4419-1417-0.

[26] R. Storn, K. Price, J. Lampinen, *Differential Evolution - A practical Approach to Global Optimization*, ACM Computing Classification (1998) Springer ISBN 3-540-20950-6